JOURNAL OF GEOPHYSICAL RESEARCH, VOL. 103, NO. A10, PAGES 23,677-23,690, OCTOBER 1, 1998

Solar wind acceleration by large-amplitude nonlinear waves: Parametric study

L. Ofman[1] and J. M. Davila
Laboratory for Astronomy and Solar Physics, NASA Goddard Space Flight Center
Greenbelt, Maryland

Abstract. We investigate the parametric dependence of the solar wind acceleration by large-amplitude nonlinear (LAN) magnetohydrodynamic waves. For this purpose we model numerically the self-consistent problem of the solar wind with waves by solving time-dependent, nonlinear, resistive 2.5-dimensional (three-dimensional with azimuthal symmetry) MHD equations driven by Alfvén waves. We find that when the Alfvén wave amplitude is above a parameter-dependent threshold, LAN waves are generated in the model coronal hole. For typical coronal parameters the solar wind speed and density fluctuate considerably on a timescale of ~10-40 min and with an amplitude of up to several hundred kmilometers per second near the Sun ($r \lesssim 10\ R_S$) in agreement with recent interplanetary scintillation observations. The solar wind speed is inversely dependent on the driving frequency in the range 0.35-3 mHz. The amplitude of the velocity fluctuations increases with the amplitude of the magnetic field and the driving Alfvén waves at the base of the corona and decreases with the coronal temperature. We found that for the same typical solar wind and Alfvén wave parameters and an isothermal initial atmosphere, the WKB model predicts 30% higher flow velocities far from the Sun (32 R_S) than our self-consistent wave model with high-frequency Alfvén waves ($f = 2.78$ mHz), conforming to the WKB approximation. However, our model predicts significantly higher average flow speed near the Sun. When low-frequency non-WKB waves drive the wind, our model predicts 25% higher solar wind speed than the WKB model far from the Sun. This result of our model is in agreement with linear studies of solar wind acceleration by Alfvén waves that take into account Alfvén wave reflection.

1. Introduction

Coronal hole regions are well-known sources of high-speed solar wind [*Krieger et al.*, 1973; *Neupert and Pizzo*, 1974; *Wagner*, 1976; *Nolte et al.*, 1976]. Recently, the Ulysses spacecraft has encountered continuous fast solar wind in the range 700-800 km s^{-1} above the polar coronal holes at a distance of ~1.6 AU [*Phillips et al.*, 1995]. Thermal conduction alone is not sufficient to explain the observed flow speed of the high-speed streams [e.g., *Kopp and Holzer*, 1976; *Holzer and Leer*, 1980; *Leer and Holzer*, 1980; *Davila*, 1985].

To account for the observed properties of the solar wind, Alfvén waves were suggested as a source of momentum and heat and studied in the linear regime [e.g., *Alazraki and Couturier*, 1971; *Belcher*, 1971; *Hollweg*, 1973; *Jacques*, 1977; *Davila*, 1985; *Davila*, 1987; *An et al.*, 1990; *Hollweg*, 1990; *Barnes*, 1992; *Velli*, 1993; *MacGregor and Charbonneau*, 1994; *Ofman and Davila*, 1995]. The WKB approximation is the standard approach to study the effect of the Alfvén waves on the solar wind. Recent linear models include many realistic features and consider the propagation of three-dimensional Alfvén waves in a stratified, thermally conductive solar wind with WKB and non-WKB approximations [*Lou*, 1993a; *Velli*, 1993; *Orlando et al.*, 1996; *Orlando et al.*, 1997]. Alfvén waves were also suggested as the driving mechanism for stellar winds in late type stars [e.g., *Belcher and Olbert*, 1975; *Heinemann and Olbert*, 1980; *An et al.*, 1990; *Lou and Rosner*, 1994; *Charbonneau and MacGregor*, 1995].

Interplanetary scintillation (IPS) observations suggest that the solar wind has a transient and dynamical nature, with large spatial and temporal inhomogeneities on angular scales of a few degrees or less (subtended at the Sun) in the first ~0.1 AU from the Sun [*Andreev et al.*, 1996; *Grall et al.*, 1996; *Klinglesmith*, 1996; *Misawa and Kojima* 1996]. IPS observations find that a peak-to-peak velocity range is up to 900 km s^{-1} at 10 R_S [*Klinglesmith*, 1996] and that the fluctuations de-

[1]Also at Raytheon STX Corporation, Lanham, Maryland

Paper number 98JA01996.
0148-0227/98/98JA-01996$09.00

crease with the distance from the Sun. Ulysses observations show a remarkably steady solar wind flow at a much larger distance of 1.6-4 AU In qualitative agreement with these observations, we show with the 2.5-dimensional (three-dimensional with azimuthal symmetry) MHD model that when large-amplitude nonlinear (LAN) waves are present the solar wind speed and density fluctuate considerably, in addition to the Alfvénic fluctuations close to the Sun.

In order to consider fully the solar wind acceleration by transverse Alfvén waves, nonlinear effects must be included. This is necessary in order to couple the transverse motions and the gradients of the magnetic pressure into the longitudinal motions. A nonlinear two-fluid one-dimensional MHD solar wind model with WKB Alfvén waves was developed by *Esser et al.* [1986] and compared favorably with observations [*Esser et al.*, 1997]. However, with the WKB approach the Alfvén waves are not treated self-consistently with the solar wind. Nonlinear effects due to the Alfvén waves in the solar wind, such as fast and slow waves, were deduced from the second-order analysis of the MHD equations [*Lou*, 1993b]. Recently, self-consistent nonlinear computations of the solar wind acceleration by Alfvén waves were performed in one spatial dimension [*Lau and Siregar*, 1996; *Boynton and Torkelsson*, 1996] and in two dimensions [*Ong et al.*, 1997; *Ofman and Davila*, 1997a].

Ofman and Davila [1997a] (hereafter referred to as OD97) investigated the self-consistent nonlinear effects due to Alfvén waves in coronal holes via numerical solution of the nonlinear 2.5-dimensional resistive MHD equations in a spherical geometry with an (r, θ) inhomogeneous atmosphere and the hydrostatic initial state. They found that solitary waves are driven by the Alfvén waves in a stratified coronal hole. *Ofman and Davila* [1997b] suggested that the solitary waves may explain the apparent broadening of ion emission lines observed by the SOHO ultraviolet coronagraph spectrometer (UVCS).

The nonlinear waves that OD97 found propagate in a highly inhomogeneous radially divergent, dispersive, and dissipative medium. These waves consist of longitudinal (sound-like) and perpendicular (Alfvénic) components. The waves are solutions of the nonlinear time-dependent 2.5-D MHD system of equations and are considerably more complex than the ideal solitary waves. Therefore we use the more general term "LAN waves" in the present study. The LAN waves resemble sound solitons in their propagation and their relation between the phase speed and amplitude. The LAN waves form when the steepening of longitudinal sound waves, driven by the Alfvén waves, is balanced by dispersive and dissipative effects in the inhomogeneous coronal hole structures. The properties of the LAN waves are determined by the radial and the transverse structure of the coronal hole, and their amplitude varies with radial distance. These waves, acting on a hydrostatic initial condition, may accelerate the solar wind to supersonic velocities.

In the present study we extend the OD97 model by using more realistic initial state and parameters and investigate the parametric dependence of the LAN waves. We use a numerical technique and geometry similar to OD97, replacing the hydrostatic initial state with *Parker's* [1963] isothermal solar wind solution and with more complex initial magnetic field. In particular, we find that low-frequency Alfvén waves with a period of about an hour drive LAN waves in the radial flow velocity, which contributes significantly to the acceleration of the solar wind in coronal holes such that the fluctuating solar wind speed at 32 R_S agrees with the observed fast solar wind speed of 500-900 km s^{-1} [*Grall et al.*, 1996]. The dynamical evolution and the spatial variability of the LAN wave driven wind are in better qualitative agreement with observations than the slowly varying, thermally driven and WKB Alfvén wave solar wind models (for a review of recent models and observations, see *Winterhalter et al.* [1996]).

We explore the parametric dependence of the solar wind outflow velocity and its fluctuations on the physical parameters of the coronal hole. Since the exact values of the parameters such as the magnetic field strength, temperature, and wave amplitude in the solar corona are presently not known, the results of the present model could be used as a guide for observation. In addition, the known dependence of the model on the parameters will allow us to test the model when new observations become available.

2. Model Equations and Boundary Conditions

We solve the normalized resistive MHD equations with the usual notation for the variables [see, for example, *Usmanov*, 1993]

$$\frac{\partial \rho}{\partial t} + \nabla \cdot (\rho \mathbf{v}) = 0, \tag{1}$$

$$\frac{\partial \mathbf{v}}{\partial t} + (\mathbf{v} \cdot \nabla)\mathbf{v} = -\frac{E_u}{\rho}\nabla p - \frac{1}{F_r r^2} + \frac{\mathbf{J} \times \mathbf{B}}{\rho}, \tag{2}$$

$$\frac{\partial \mathbf{B}}{\partial t} = \nabla \times (\mathbf{v} \times \mathbf{B}) + S^{-1}\nabla^2 \mathbf{B}, \tag{3}$$

$$\left(\frac{\partial}{\partial t} + \mathbf{v} \cdot \nabla\right)\frac{p}{\rho^\gamma} = 0. \tag{4}$$

The normalization in equations (1)–(4) is the following: $r \rightarrow r/R_S$, $t \rightarrow t/\tau_A$, $v \rightarrow v/v_A$, $B \rightarrow B/B_0$, $\rho \rightarrow \rho/\rho_0$, and $p \rightarrow p/p_0$. In the above, R_S is the solar radius, $\tau_A = R_S/v_A$ is the Alfvén time, $v_A = B_0/\sqrt{4\pi\rho_0}$ is the Alfvén velocity, B_0 is the magnetic field, ρ_0 is the density, and p_0 is the pressure at the center of the coronal hole at $r = 1$. Other physical parameters are the Lundquist number S (in the present study, $S = 10^4$), the Froude number $F_r = v_A^2 R_S/(GM_S)$, where G is the gravitational constant and M_S is the solar mass, and the Euler number $E_u = p_0/(\rho_0 v_A^2) = c_s^2/\gamma v_A^2$,

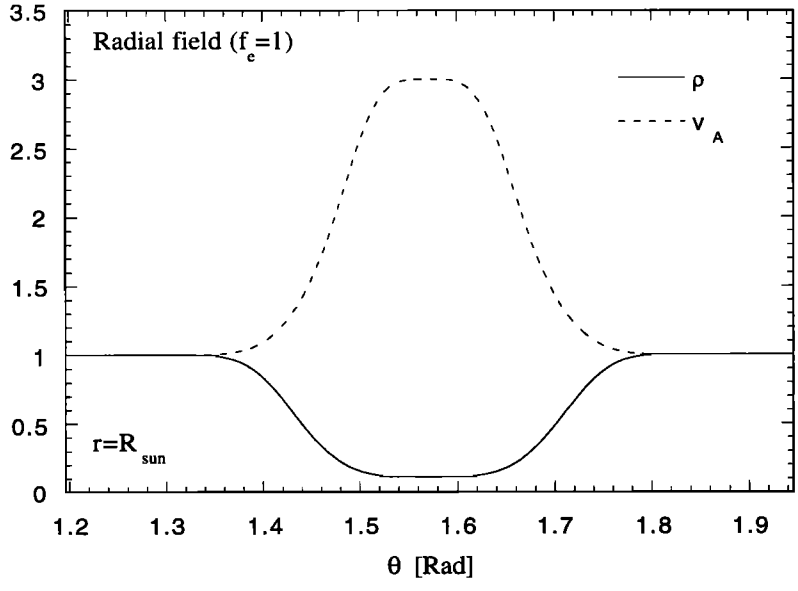

Figure 1. The θ dependence of the initial density and the Alfvén velocity for the radial magnetic field case ($f_e = 1$).

where c_s is the sound speed. With this normalization, $\beta = 8\pi p_0/B_0^2 = 2E_u$.

In the present study we assume that the plasma is isothermal, i.e., $\gamma = 1$. This assumption implies a significant energy input into the coronal plasma. However, this energy is not sufficient to accelerate the solar wind to the fast solar wind speed of 800 km s^{-1} deduced from observations. The *Parker* [1963] isothermal solar wind speed is about 420 km s^{-1} at 32 R_S and about 600 km s^{-1} at 215 R_S (Earth's orbit).

The isothermal assumption, together with the ideal gas law, implies that the pressure is proportional to the density. Thus we do not need to solve the energy equation explicitly, and we can substitute ρ for p in the normalized momentum equations.

To relax the isothermal assumption, one can use the polytropic solar wind solution [*Parker*, 1963] with $\gamma = 1.05$, a commonly used value [e.g., *Linker et al.*, 1990; *Mikić and Linker*, 1996]. With $\gamma = 1.05$ the calculated solar wind velocity is close to the isothermal solar wind flow. For example, at 32 R_S the solar wind velocity is $v_r = 390$ km s^{-1}, which is somewhat lower than the $v_r = 420$ km s^{-1} of the isothermal model. Note that with $\gamma = 1.05$ the temperature at 32 R_S is about 60% of the value at the base of the coronal hole. We have tested our model with $\gamma = 1.05$ and found acceleration similar to the isothermal model.

For the radially divergent initial magnetic field configuration $\mathbf{B}_0 = B_0 r^{-2}\mathbf{e}_r$ the simulations are initiated with the background density profile

$$\rho_0(r,\theta) = \left[1 - (1-\rho_r)\, e^{-[(\theta-\pi/2)/\theta_s]^4}\right] \rho(r)/\rho_r, \quad (5)$$

where $\rho_r = \frac{1}{9}$ and θ_s determines the angular extent of the low-density region in the center of the coronal hole (in the present study we use $\theta_s = 0.15$, unless indicated otherwise; see Figure 1). The radial dependence of the density and the radial component of the solar wind velocity v_r are initialized with the *Parker* [1963] isothermal solar wind solution (see Figure 2).

To compare our results with one-dimensional studies we use the following definition of the maximal divergence rate at $\theta = \pi/2$ (the symmetry axis of the coronal hole):

$$f_e = \max\left\{\frac{B(1)}{B(r)r^2}\right\}. \quad (6)$$

With the radial magnetic field the above expression yields $f_e = 1$. For non-radial divergence a quadrupole field is added to the radial field

$$\mathbf{B} = \left[\frac{B_0}{r^2} - \frac{3B_4(3\cos^2\theta - 1)}{2r^4}\right]\mathbf{e}_r - \frac{3B_4 \sin 2\theta}{2r^4}\mathbf{e}_\theta. \quad (7)$$

By choosing appropriate values of the parameters B_0 and B_4 one can set the desired value of f_e and the magnetic field strength at the center of the coronal hole B(1,π/2). We use $B_0 = 0.1$ and $B_4 = 0.6$ to get $f_e = 10$ and B(1,π/2)=1. For the nonradial field case the θ dependence of the initial density structure is determined from magnetic and thermal pressure balance in θ (since $\rho \propto p$ in an isothermal plasma). The θ dependence of the density, the magnetic field, and the Alfvén velocity at $r = 1$ are shown in Figure 3. At $r = 1$ the Alfvén velocity peaks at the center of the coronal hole and flattens toward the boundaries. The B_{r0} component of the magnetic field is symmetric, and $B_{\theta 0}$ is antisymmetric with respect to the center of the model coronal hole.

We use the following boundary conditions at $r = 1$ to generate Alfvén waves (see OD97 for more details): $B_\phi(1,\theta) = v_d/v_A(1,\theta)\cos\omega t$, with $B_r(1,\theta) = B_{r,0}$ and $v_\theta(1,\theta) = B_\theta(1,\theta) = 0$; and $v_r(1,\theta) \geq 0$, where v_d is the

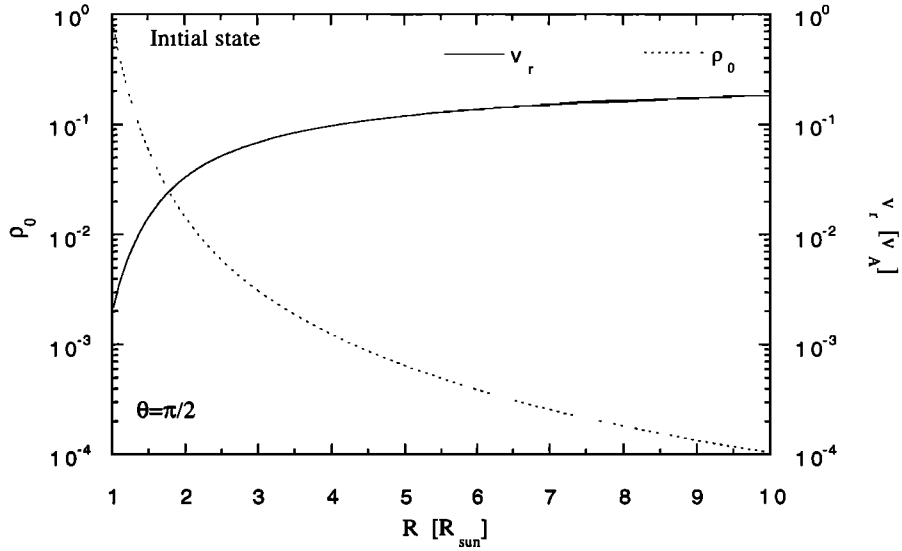

Figure 2. The r dependence of the initial density and the radial velocity at $\theta = \pi/2$

driving Alfvén wave amplitude in units of v_A and ω is the driving frequency in units of τ_A^{-1}. Below, f denotes the frequency in physical units. The boundary conditions for the remaining variables are determined by approximating the incoming characteristic equations with extrapolation of the variables from the internal region to the boundary [*Steinolfson and Nakagawa*, 1976].

At $\theta = \pi/2$ we assume symmetry and solve the 2.5-D MHD equations in the domain $(\pi/2, \pi/2 + \theta_0) \times (1, r_{\max})$, where $r_{\max} = 10$-40. We use the Runge-Kutta method with fourth-order accuracy in time and in space. In addition, a fourth-order smoothing term (i.e., numerical viscosity) and upwind differencing of the density are used to stabilize the method. Up to 64×4096 uniform grid points are used (high-frequency, $r_{\max} = 40$), with 64×1024 in most cases. The adjustable time step was determined by the Courant-Friedrichs-Lewy (CFL) condition.

In order to test our code we compared the solution for small-amplitude Alfvén waves in a hydrostatic background atmosphere with the solutions of the spherical Alfvén wave equation (equation (14) in the appendix) and found a very good agreement. Since equation (14) does not include dissipation, it is possible to calculate the effect of the dissipation in our code by comparing the decrease of the amplitude of the Alfvén waves with r to the ideal solutions. We find that when $S = 10^4$ the effects of the dissipation close to the Sun ($r < 10\ R_S$) are negligible. At larger distances the amplitude of the high-frequency Alfvén waves decreases significantly, and

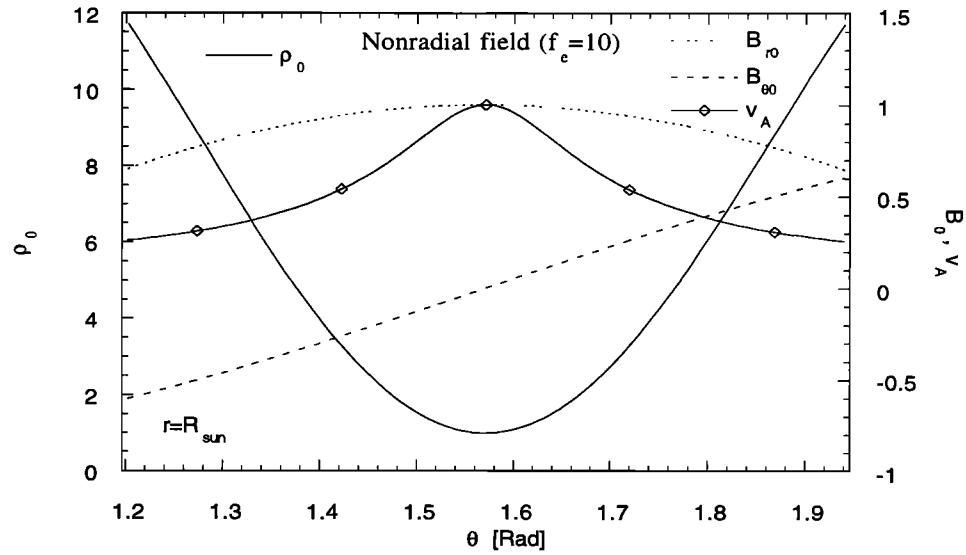

Figure 3. The θ dependence of the initial density and the magnetic field components for the nonradial case ($f_e = 10$).

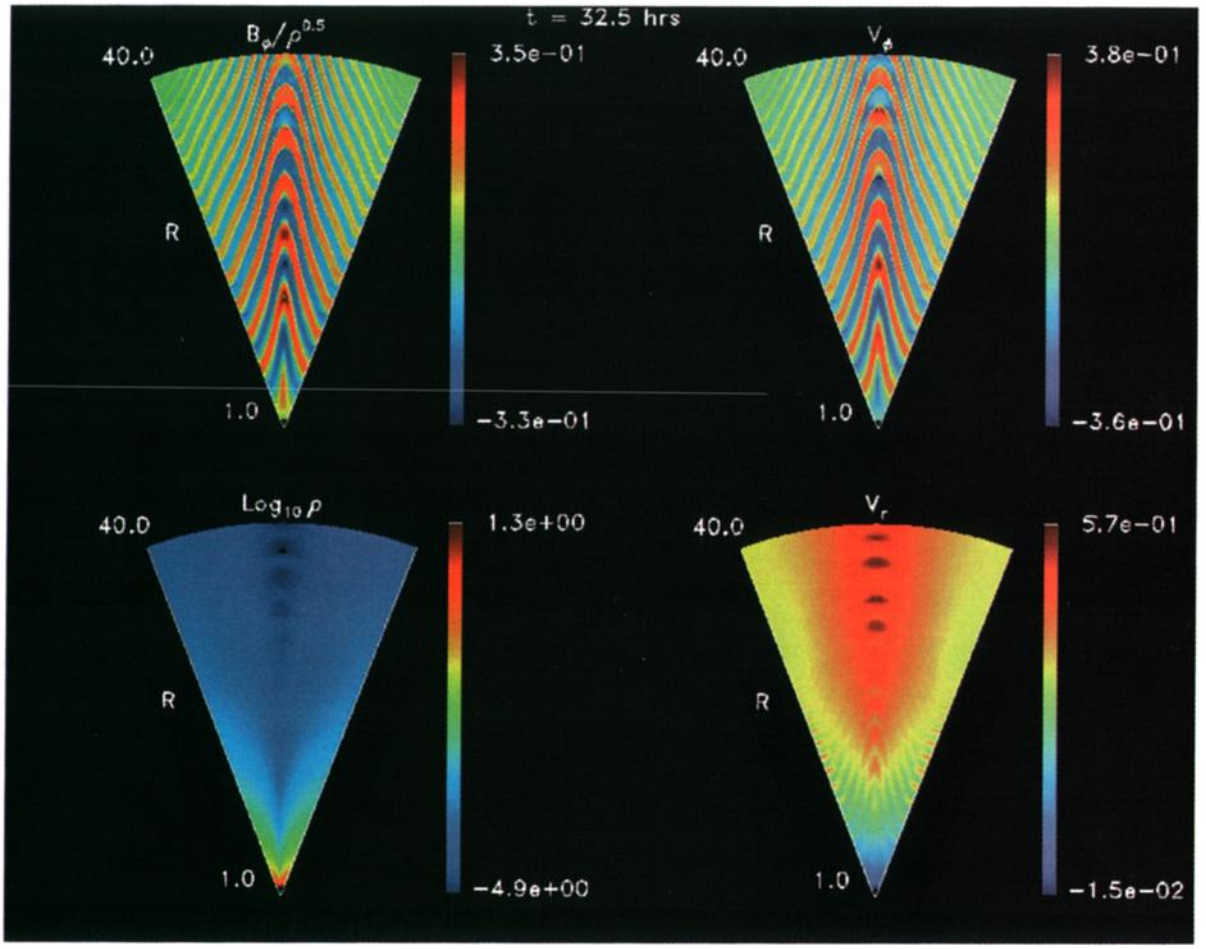

Plate 1. The result of a run of the coronal hole model with the parameters $v_d = 46$ km s^{-1}, $B_0 = 7$ G, $T = 1.4 \times 10^6$ K, $f = 0.35$ mHz, $n_0 = 10^8$ cm^{-3}, and $f_e = 10$. The spatial dependence of $B_\phi/\rho^{0.5}$, v_ϕ, v_r, and ρ are given at $t = 255\tau_A = 32.5$ hours. The velocities and $B_\phi/\rho^{0.5}$ are in units of the Alfvén speed (1527 km s^{-1}), and the density is in units of 10^8 cm^{-3}. The nonlinear waves are evident in v_r and ρ (with inphase fluctuations). The Alfvén waves are evident in v_ϕ and $B_\phi/\rho^{0.5}$ that are 180° out of phase.

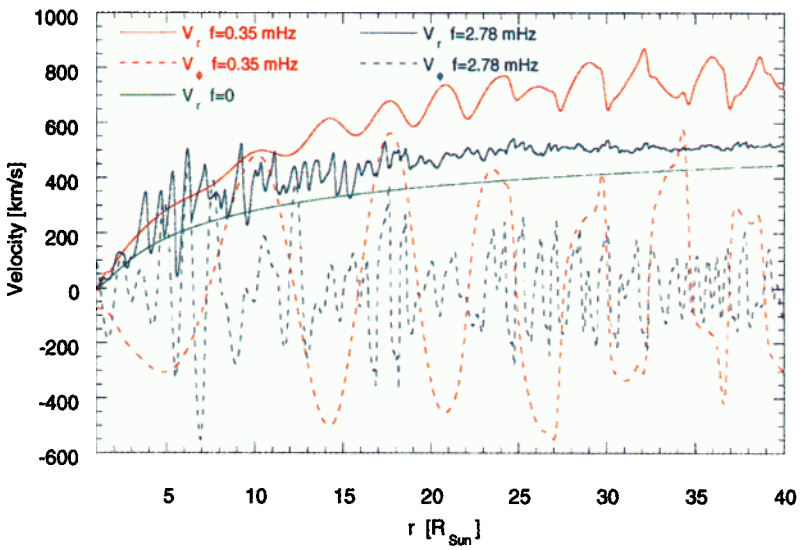

Plate 2. The radial dependence of the solar wind velocity components v_ϕ and v_r at the center of the coronal hole for the case in Plate 1, and for the run with $f = 2.78$ mHz. For reference, *Parker*'s [1963] solar wind solution without waves ($f = 0$) is shown.

at $r = 32\ R_S$ is about 20% below the dissipationless value. Thus, in the ideal limit, the nonlinear effects would appear stronger. However, the Alfvén wave dissipation in the model has little effect on the solar wind acceleration since most of the acceleration takes place closer to the Sun. We have investigated the scaling of the dissipation and phase-mixing of Alfvén waves with S and f in Cartesian geometry in an earlier study [*Ofman and Davila*, 1995].

3. Numerical Results

In Figures 1-10 and Plates 1 and 2 we present the results of the parametric studies of the solar wind radial velocity and the velocity fluctuation. During the simulation run the maximal v_r and δv_r were found at an "observation" point ($\theta = \pi/2$, r) in the coronal hole after the solution achieved a quasi steady state. We show the solar wind velocity far ($r = 32\ R_S$) from the Sun, where the average solar wind speed is nearly level in r. We also show results close to the Sun ($r = 5.9\ R_S$, $8.2\ R_S$) in order to investigate the effect of the waves on the acceleration in the near-solar region.

The simulations were run until the magnitude of the velocity and the magnetic field reached a quasi steady state. In most cases the amplitude of δv_r and of other variables varied in time even at the "steady" state phase of the simulations due to the presence of higher harmonics and the interactions between these harmonics (see OD97). The values of δv_r shown in Figures 1-10 and Plates 1 and 2 were obtained by averaging several wave amplitudes near the peak amplitude. In the following sections we investigate the effects of various parameters on the solar wind velocity (in each case the indicated parameters are varied while the rest remain fixed).

In Plate 1 we show the results of a run of the coronal hole model with the parameters $v_d = 46$ km s^{-1}, $B = 7$ G, $T = 1.4 \times 10^6$ K, $f = 0.35$ mHz, the number density at the base of the coronal hole $n_0 = 10^8$ cm^{-3}, and an expansion ratio $f_e = 10$. The spatial dependence of $B_\phi/\rho^{0.5}$, v_ϕ, v_r, and ρ are given at $t = 255\tau_A = 32.5$ hours. The nonlinear waves are evident in v_r and ρ, with highest amplitude near the center of the coronal hole (see Plates 1-2 and Figure 4). The Alfvén waves are evident in v_ϕ and in $B_\phi/\rho^{0.5}$ that are 180° out of phase, as expected for traveling Alfvén waves. In the present study we use a single-frequency driver to generate the Alfvén waves. The period of the density fluctuations that we obtained from the present run is about 45 min with $f = 0.35$ mHz (~15 min with $f = 2.78$ mHz and radial field). These values are longer than what would be expected for second-order fluctuations (23.8 min for $f = 0.35$ mHz and 3 min for $f = 2.78$ mHz) and depend on the period of the Alfvén waves that drive the nonlinear waves in the model and on other coronal hole parameters. The frequency of the LAN waves increases with f. In the solar corona we expect that a spectrum of frequencies will be present in the Alfvénic fluctuations and that the resulting temporal (and spatial) spectrum of the LAN waves will be more complex than in the present model.

In Plate 2 we show the radial dependence of the solar wind velocity components v_r and v_ϕ at the end of the run shown in Plate 1. For comparison, we also show the results of a run with $f = 2.78$ mHz, $f_e = 1$, and the *Parker* [1963] isothermal solar wind solution. In Plate 2

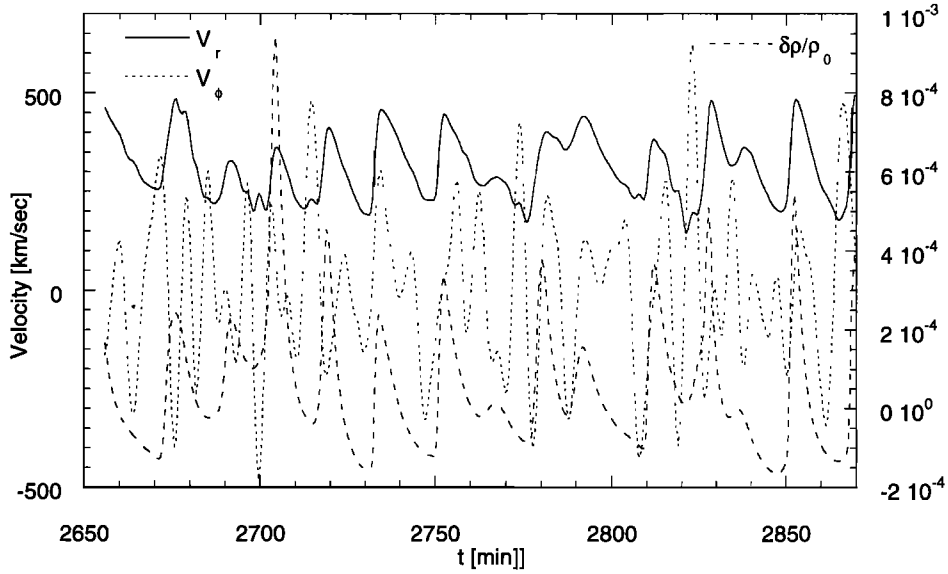

Figure 4. The time dependence of v_r, v_ϕ, and $\delta\rho/\rho_0$ at $r = 7\ R_S$ in the center of the coronal hole for the case with $f = 2.78$ mHz in Plate 2.

the relation between v_r and v_ϕ is more apparent. It is evident that for the 0.35-mHz case the dominant wavelength in v_r is half the wavelength of v_ϕ near the Sun. Far from the Sun ($r \gtrsim 25\ R_S$) the structure of the waves becomes more complex due to nonlinear steepening, balanced by dispersion and dissipation. The wave fronts steepen into shocks in the region $r > 25\ R_S$, However, the average solar wind speed does not vary significantly with r in that region.

Since the steepening of the wave fronts is limited by the numerical dissipation, one must investigate its effect on the calculated solar wind speed. To test the effect of the numerical dissipation, we have doubled and halved the resolution in the radial direction. We found that the width of the shock fronts is proportional to the resolution, i.e., numerical viscosity. However, the average solar wind speed and the amplitude of the LAN waves are not significantly affected.

When the wind is accelerated by the high-frequency Alfvén waves, the nonlinear steepening occurs closer to the Sun ($r \gtrsim 5\ R_S$) than with the low-frequency waves. In Figure 4 we show the temporal evolution of v_r, v_ϕ, and $\delta\rho/\rho_0$ at $r = 7\ R_S$ in the center of the coronal hole for the case with $f = 2.78$ mHz discussed above. It is evident that the fluctuations of the density and the velocity are in phase. When the fluctuations of v_r are averaged out, the resulting solar wind speed is higher than the solar wind speed without waves (i.e., *Parker*'s [1963] solution) at the same radial distances.

We have calculated the power spectrum of the velocity components using the fast Fourier transform (FFT). From the wavelength and frequency of v_r we have determined the phase speed of the LAN waves. We found that the phase speed at $r = 7\ R_S$ is about 400 km s^{-1}. This speed is above the local average solar wind ($\sim$ 300 km s^{-1}) and below the local Alfvén speed ($\sim$ 1500 km s^{-1}).

We have looked at the various terms in the radial component of the momentum equation as a function of the radial distance and time. We found that the acceleration due to the Alfvén waves $(B_\phi/\rho)(\partial B_\phi/\partial r)$ in the Lorenz force and the acceleration due to the LAN waves $v_r(\partial v_r/\partial r)$ in the Reynolds stress are of comparable magnitude in most of the coronal hole except close to the Sun ($r > 2\ R_S$ for $f = 2.78$ mHz; $r > 10\ R_S$ for $f = 0.35$ mHz). Close to the Sun the thermal pressure gradient is the dominant force.

3.1. The Dependence of v_r and δv_r on Perpendicular Structure Parameter θ_s

In Figure 5 we show the dependence of v_r and δv_r on θ_s (the half-angular width of the low-density region) in the coronal hole at $r = 5.9\ R_S$, with $B = 7$ G, $T = 1.4 \times 10^6$ K, $v_d = 38.2$ km s^{-1}, $f = 3.33$ mHz, and $S = 10^3$. When θ_s is small (0.05 radians) the amplitude of δv_r is about 15 km s^{-1} and $v_r \approx 260$ km s^{-1}. When θ_s is increased to 0.375 radians, δv_r reaches about 300 km s^{-1} and $v_r \approx 460$ km s^{-1} at the center of the coronal hole.

The scale of the perpendicular gradients of the density profile is determined by θ_s in equation (5). When θ_s is small, the density is near the maximal density over most of the simulation region. The Alfvén velocity and the energy density of the input Alfvén waves are lower than for larger θ_s for the same v_d and f. When θ_s is increased, the input energy flux and the amplitude of the nonlinear waves increase. It is evident that this wave energy is carried across the coronal hole since the background density, the magnetic field, and the Alfvén wave amplitude do not change in the center of the coronal hole when θ_s is varied. Thus the structure of the coronal hole density across the field determines the magnitude of the solar wind at the center of the coronal hole.

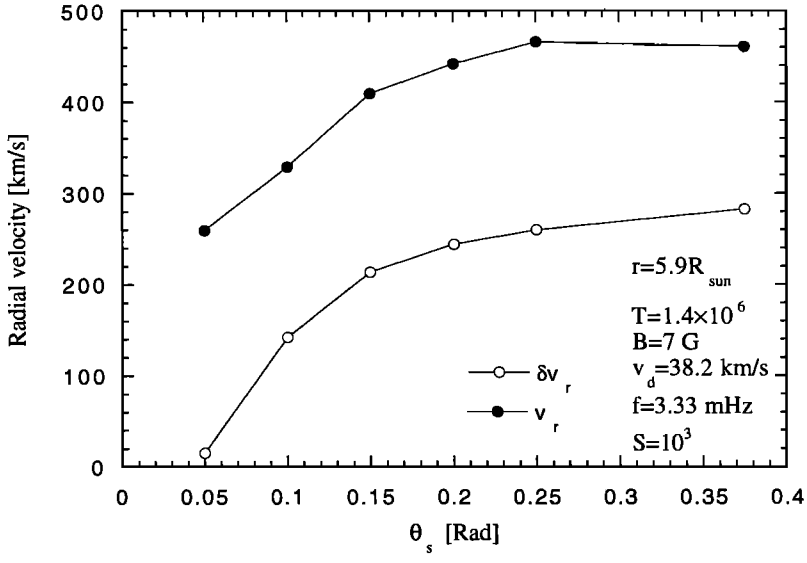

Figure 5. The dependence of the radial velocity and its fluctuation amplitude on the angular width of the low-density region of the coronal hole.

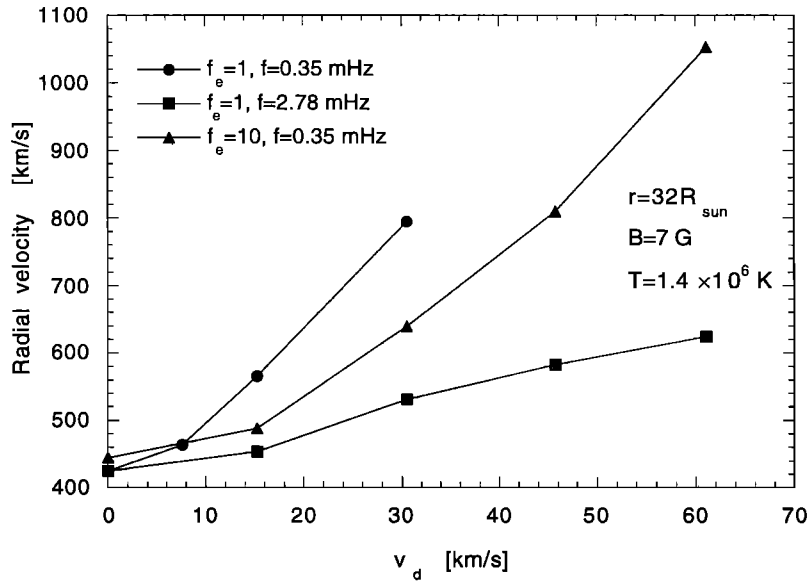

Figure 6. The dependence of the radial velocity on the amplitude of the Alfvén waves for radial (with f=0.35, 2.78 mHz) and superradial (with f=0.35 mHz) background magnetic field.

3.2. The Dependence on the Driving Alfvén Wave Amplitude v_d and the Divergence f_e

In Figure 6 we show the results of the study of the maximal solar wind velocity dependence on the driving amplitude of the Alfvén waves at the base of the coronal hole for radially divergent (f_e = 1) and superradial (f_e = 10) magnetic field structure. The velocity is shown at a distance of r = 32 R_S, where the solar wind acceleration is small. When v_d = 0, *Parker*'s [1963] solar wind speed is recovered. With the superradial magnetic field divergence the solar wind speed is 800 km s^{-1} (i.e., typical fast solar wind value) at 32 R_S with a reasonable coronal Alfvén wave amplitude of $v_d \approx$ 46 km s^{-1} [*Hassler et al.*, 1990]. When the radial magnetic field configuration is used as an initial state with f = 0.35 mHz, the solar wind speed reaches 800 km s^{-1}, with an even lower driving amplitude of v_d = 30 km s^{-1}.

We show below that the solar wind speed increases when the driving frequency decreases (see Figure 8). To show this effect in a radially divergent coronal hole, we have included a study of the solar wind speed dependence on v_d for the higher-frequency (f = 2.78 mHZ) driving Alfvén waves. It is evident that with the higher driving frequency the solar wind speed does not reach 800 km s^{-1} with reasonable v_d and remains below the typical fast solar wind speed.

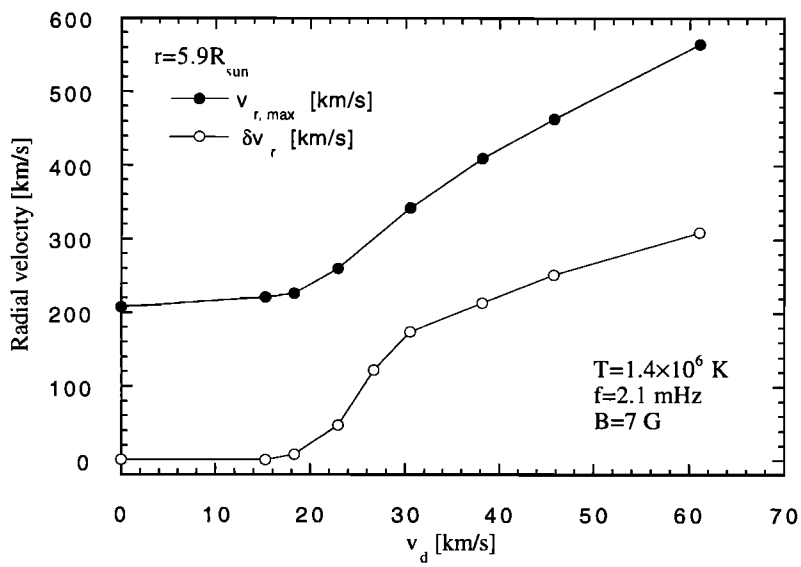

Figure 7. The dependence of the radial velocity and its fluctuation amplitude on v_d close to the Sun (5.9 R_S).

To investigate the effect of v_d on solar wind acceleration close to the Sun, we show in Figure 7 the dependence of v_r and δv_r on v_d at 5.9 R_S. The other parameters are $f = 2.1$ mHz, $B = 7$ G, and $T = 1.4 \times 10^6$ K. When $v_d < 20$ km s^{-1} the solar wind speed flows at the *Parker* [1963] isothermal solar wind velocity of about 200 km s^{-1}. When v_d is increased, both v_r and δv_r increase. When $v_d \approx 60$ km s^{-1}, the solar wind speed is about 600 km s^{-1} and $\delta v_r \approx 300$ km s^{-1}.

In Figure 7 it is evident that for v_d above ~30 km s^{-1} the solar wind velocity increase is dominated by the LAN waves. Above that threshold the solar wind speed and the fluctuations increase linearly with v_d. The phase speed of the LAN waves is much lower than the Alfvén speed near the Sun and are given approximately by the sound speed plus the average solar wind speed. Below the transition threshold, the solar wind fluctuations are small and are dominated by the second-order waves that propagate at an Alfvén phase speed. The second-order fluctuations increase nearly quadratically with v_d.

3.3. The Effect of the Driving Frequency f and the Field B

The dependence of v_r and δv_r on f for several values of $B = B(r = 1, \theta = \pi/2)$ is explored in Figure 8. The observation point is at 32 R_S, and $\theta = \pi/2$. The magnetic field is $B = 5$, 7, and 10 G, $v_d = 30.5$ km s^{-1}, and $T = 1.4 \times 10^6$ K. The *Parker* [1963] solar wind speed at 32 R_S for this temperature is 425 km s^{-1}. It is evident that the solar wind with waves reaches significantly higher speed than the wind without waves with the same physical parameters. When $f > 2$ mHz, the fluctuations of the solar wind velocity are small. When f is decreased and B is increased, both v_r and δv_r increase. When $B = 10$ G and $f = 0.35$ mHz, the maximal solar wind speed at 32 R_S reaches the typical fast solar wind speed value of 800 km s^{-1}.

The increase in the solar wind speed when f is decreased can be understood from the linear solutions for the Alfvén waves (see the appendix, and *Lou and Rosner* [1994] and *Orlando et al.* [1996]). When the wavelength of the driving Alfvén waves is small compared with the background Alfvén velocity gradients ($f > 2$ mHz), the Alfvén waves are in the WKB regime and their amplitude can be found from equation (8). When the wavelength of the Alfvén waves is comparable or larger than the background Alfvén velocity gradients ($f < 2$ mHz), non-WKB effects such as reflection become important, and the velocity amplitude of the Alfvén waves increases (see Figure 10). The increase in the Alfvén velocity amplitude leads to stronger nonlinearity and to an increase of the LAN wave amplitude. This results in larger v_r and δv_r for small f in Figure 8.

3.4. The Effect of the Coronal Temperature T and the Field B

The dependence of the maximal solar wind speed at $r = 8.2$ R_S on the coronal temperature with $B = 5$ and 10 G, $f = 3.33$ mHz is shown in Figure 9. Since the sound speed is proportional to $T^{0.5}$ and the nonlinearity appears as a compressional wave, we set the driving Alfvén wave amplitude at the base to $v_d = 0.2c_s$. The amplitude of the maximal solar wind velocity increases when the temperature decreases from 1.8×10^6 K to 1.1×10^6 K. The decrease in temperature leads to an increase of the radial density gradient that increases the background Alfvén velocity radial gradient. The larger radial gradient in the background Alfvén velocity leads to an increase of the Alfvén wave amplitude as it propagates outward, which couples to the nonlinear radial velocity amplitude. When the magnetic field strength

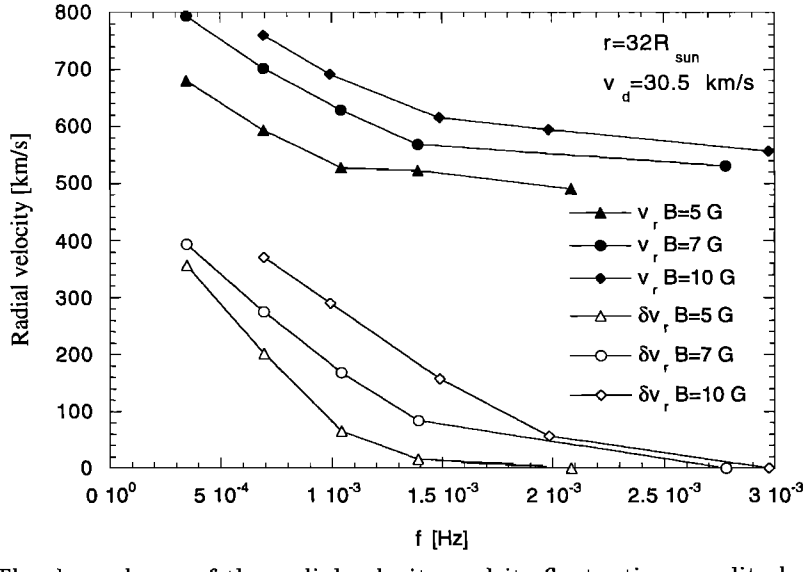

Figure 8. The dependence of the radial velocity and its fluctuation amplitude on the driving Alfvén wave frequency for $B = 5$, 7, and 10 G.

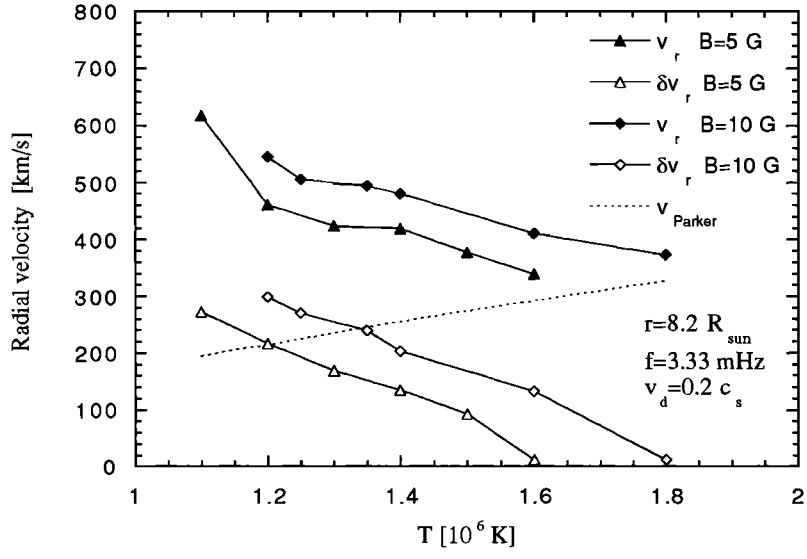

Figure 9. The dependence of the radial velocity and its fluctuation amplitude on the background coronal temperature for $B = 5$ and 10 G at $r = 8.2\ R_S$. *Parker*'s [1963] isothermal solar wind velocity (i.e., without waves) for the same T and r is shown by the dashed line.

at the base of the corona is increased (the density and other parameters being fixed), the energy input of the Alfvén waves increases, and the amplitude of v_r and δv_r accordingly increases.

The amplitude of δv_r at $r = 8.2\ R_S$ was found to increase when the temperature decreases in the computational range $T = 1.1 - 1.8 \times 10^6$ and with $B = 5$ and 10 G. For example, when $B = 5$ G and $T = 1.8 \times 10^6$ K, the value of δv_r at 8.2 R_S is several kilometers per second and increases to about 270 km s^{-1} when the temperature is lowered to $T = 1.1 \times 10^6$ K. For this low temperature the maximal solar wind velocity is more than 3 times the *Parker* [1963] solar wind velocity for the same r and for the same temperature.

4. Discussion and Conclusions

In the present study we explore the parametric dependence of the solar wind acceleration by nonlinear magnetohydrodynamic waves. We have modeled numerically the solar wind acceleration by solving the time-dependent, nonlinear, resistive 2.5-dimensional MHD equations driven by Alfvén waves. We find that when the Alfvén wave amplitude is above a parameter-dependent threshold, LAN waves are generated in the radial outflow velocity and density. The forces exerted by these waves on the solar wind (with the dominant force due to $\frac{1}{2}(\partial(v_r^2)/\partial r)$ in the momentum equation) are comparable in magnitude to the Alfvén wave pressure.

The main new results of the present study are the quantitative dependence of v_r and δv_r on v_d, f, T, B, and θ_s for realistic coronal parameters. Since the exact values of the above parameters in the solar corona are presently not known, it is important to investigate the dependence of the solar wind model on the parameters in order to find regions in the parameter space that agree with observation. In addition, various coronal hole structures (such as plumes) have different characteristic parameters and magnetic field topology. Obviously, the coronal parameters vary in time. For example, the average magnetic field strength changes with the solar cycle. Thus the results of the present study could, in principle, be applied to a particular coronal structures if its physical parameters are determined from observations.

In particular, we find that the solar wind velocity fluctuations and magnitude increase when the amplitude of the input Alfvén waves at the base of the coronal hole increases. For example, when the input Alfvén wave amplitude is 46 km s^{-1} and $f = 0.35$ mHz in a superradially divergent coronal hole, the solar wind velocity reaches the typical fast solar wind value of 800 km s^{-1}. For a radially divergent coronal hole the fast solar wind speed is reached with an even lower driving amplitude of 30 km s^{-1}. The increase in the solar wind velocity with v_d far from the Sun after a certain threshold in v_d is due to the LAN waves that become important beyond that threshold. We also find that v_r and δv_r increase when f is decreased. This effect is very significant when f is in the submillihertz range and the wave force is in the non-WKB regime.

We have compared the results of our runs with the solar wind velocity predicted by the standard one-dimensional solar wind model with WKB waves. The solar wind velocity and density profiles for the WKB solar wind model were provided to us by R. Esser [see also *Esser et al.*, 1997]. We found that for the same typical solar wind and Alfvén wave parameters and an isothermal initial atmosphere, the WKB model predicts 30% higher flow velocities at 32 R_S than our self-consistent

wave model with high-frequency Alfvén waves (i.e., conforming to the WKB approximation). However, our model predicts significantly higher average flow speed near the Sun ($r \lesssim 10\ R_S$). When low-frequency non-WKB waves drive the wind, our model predicts 25% higher solar wind speed than the WKB model far from the Sun. This result of our model is in agreement with linear studies of solar wind acceleration by Alfvén wave that take into account Alfvén wave reflection [*MacGregor and Charbonneau*, 1994].

The coronal hole temperature plays an important role in determining the nonlinear acceleration. When the temperature decreases, the density scale height decreases, increasing the radial gradients in the Alfvén velocity, which leads to higher acceleration for the same Alfvén wave frequency. For example, near the Sun ($r = 8.2\ R_S$) when the coronal hole temperature is 1.1×10^6 K, and $B = 5$ G, the maximal solar wind speed is enhanced by a factor of 3 over the standard *Parker* [1963] solar wind speed (without waves). When $T = 1.6 \times 10^6$ K, the solar wind speed is not significantly above the Parker solar wind speed.

The Alfvén waves in the present study were driven at a single frequency in each run and produced nonlinear waves with multiple harmonic spectrum (see OD97). In the solar corona it is reasonable to assume that a spectrum of the Alfvén waves will be present. This Alfvén wave spectrum will drive a complex spectrum of nonlinear waves with larger contribution from the low-frequency component of the spectrum than from higher frequencies. The nonlinear wave spectrum might resemble turbulent spectrum due to production of multiple harmonics that decrease in amplitude with frequency. We plan to study the effects of a broadband driving spectrum on the solar wind acceleration in our future papers.

It is important to remember that nonlinearly, the transverse magnetic motions are efficiently coupled to the longitudinal motions and the separation between the Alfvénic and longitudinal parts is rather artificial. The kinetic energy in the radial direction is a significant fraction of the total kinetic energy (~20% for a typical case). The LAN waves are the manifestation of this energy in the radial component of the velocity.

Helios observations at 0.29 AU show that the Alfvénic fluctuation spectrum follows a Kolmogorov-like power law in the range $10^{-4} - 10^{-2}$ Hz with the highest power in the lower frequencies [e.g., *Grappin et al.*, 1990; *Marsch and Tu*, 1990]. The spectrum appears to reach maximal power and flatten in the approximate range from 10^{-5} to 5×10^{-4} Hz [Denskat and Neubauer, 1982]. These observations support our solar wind model prediction that the submillihertz waves play an important role in the acceleration of the solar wind. The fact that the power spectrum flattens at low frequencies suggests that part of the low-frequency wave energy is transferred into solar wind acceleration.

IPS observations [*Grall et al.*, 1996; *Klinglesmith*, 1996; *Andreev et al.*, 1996] suggest that the solar wind has a transient and dynamical nature with large spatial and temporal inhomogeneities on angular scales of a few degrees or less (subtended at the Sun). According to these observations, the velocity variation is 100-200 km s^{-1} at 30 R_S and decrease farther from the Sun. In qualitative agreement with these observations, we show with the 2.5-D MHD model that when LAN waves are present the solar wind speed and density fluctuate considerably in addition to the Alfvénic fluctuations. The radial velocity fluctuations are $\delta v_r \approx$100-400 km s^{-1} in the region $10\ R_S < r < 40\ R_S$, with typical coronal hole parameters used in the model. These velocity fluctuations may have dissipated by the time the solar wind reaches distances of several hundred solar radii, since Ulysses observations show a remarkably steady solar wind flow.

Recent observations by the SOHO spacecraft (in particular the large angle and spectrometric coronagraph experiment, UVCS and extreme ultraviolet imaging telescope) further confirm that the solar wind has a transient and dynamical nature, with spatial and temporal inhomogeneities even at solar minimum. Preliminary results from the SOHO UVCS white-light channel indicate the possible presence of compressional waves near the Sun [*Ofman et al.*, 1997]. Our model shows that when LAN waves are present, the solar wind speed and density fluctuate considerably on timescales of tens of minutes and on spatial scales of 0.1-1 R_S. The spectra of the fluctuations are complex, with many harmonics induced by the nonlinear interactions of the various modes. These model predictions are in better agreement with observations than most other solar wind models that predict smooth and steady solar wind streams.

Appendix

Here we present the derivation of the Alfvén wave equation in spherical geometry in the gravitationally stratified medium. Detailed analytical and numerical study of the Alfvén wave equation in a gravitationally stratified medium was recently performed by *An et al.* [1990] and *Lou and Rosner* [1994]. The solution of the wave equation below is used to test the 2.5-D MHD code in spherical geometry.

At the base of the coronal hole the amplitude of the Alfvén waves is v_d. However, owing to spherical divergence and stratification of the density, the amplitude of the Alfvén waves increases considerably as the waves propagate into the corona. To illustrate this point we use the expression below, valid in the dissipationless, short-wavelength, small-amplitude, and static atmosphere limit. The energy flux of the Alfvén waves is constant and in a spherically symmetric case is given by

$$4\pi r^2 v_A(r) \rho \frac{\delta v(r)^2}{2} = \text{const} \qquad (8)$$

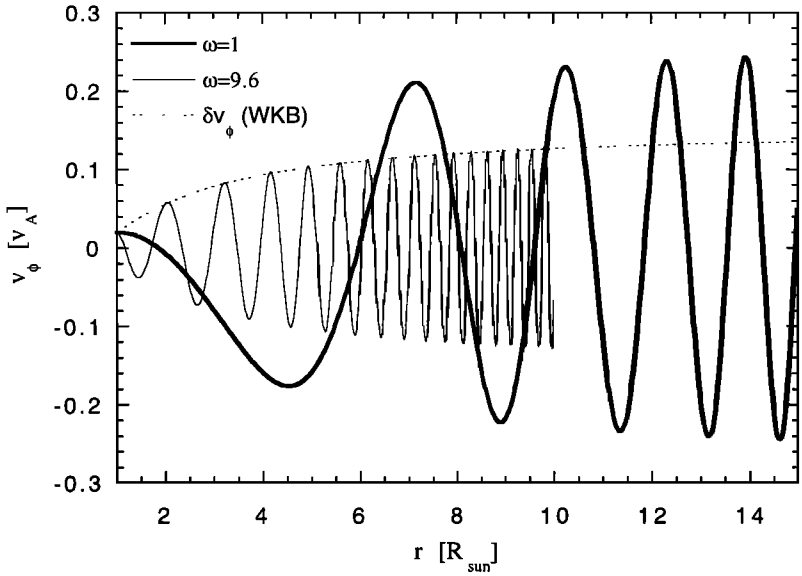

Figure 10. Solutions of the linearized Alfvén wave equation (12) in spherical geometry with gravitationally stratified atmosphere for $\omega = 9.6$ ($\Rightarrow f = 3.33$ mHz) shown for $1 \leq r \leq 10$, and $\omega = 1$ ($\Rightarrow f = 0.35$ mHz) shown for $1 \leq r \leq 15$, with $v_d = 0.02 v_A = 30.5$ km s^{-1}, $B = 7$ G, and $T = 1.4 \times 10^6$ K. The dashed line is the amplitude of the Alfvén waves obtained from equation (8).

where $v_A(r) = B(r)/\sqrt{4\pi\rho(r)}$ and $\delta v(r)$ is the Alfvén wave velocity amplitude. We have tested the validity of the above expression by launching small-amplitude Alfvén waves into an initially hydrostatic atmosphere with radial magnetic field and found an excellent agreement to 10 R_S with 300-s waves. For example, when $T = 1.3 \times 10^6$ K, the amplitude of $\delta v(r)$ increases by a factor of ~5 from $r = 1$ R_S to 7 R_S (see below). When the background solar wind is included the above expression is qualitatively valid in the first few solar radii, where v_r is small compared with $\delta v(r)$.

The Alfvén wave equation in a gravitationally stratified spherically symmetric case (i.e., $\partial/\partial\phi = \partial/\partial\theta = 0$) is derived below. We take the Alfvén waves to be linearly polarized, with $B_\theta = v_\theta = 0$. We also neglect the gradients of the thermal pressure perturbations (i.e., sound waves), background flow, and dissipation and use the radial background magnetic field $B_r = B_0/r^2$. The background density profile is calculated from the hydrostatic equilibrium density

$$\rho = e^{\alpha(\frac{1}{r}-1)} \tag{9}$$

where $\alpha = 1/(E_u F_r)$ is a function of the plasma temperature. For the Sun it is given by

$$\alpha = \frac{1.15 \times 10^7}{T}. \tag{10}$$

With the above assumptions the MHD equations (1)–(4) for Alfvén waves reduce to

$$\frac{\partial B_\phi}{\partial t} = \frac{1}{r}\frac{\partial}{\partial r}(r\, v_\phi B_r) \tag{11}$$

$$\frac{\partial v_\phi}{\partial t} = \frac{B_r}{\rho}\left(\frac{\partial B_\phi}{\partial r} + \frac{1}{r}B_\phi\right) \tag{12}$$

Taking time derivative of equation (11) and substituting into equation (12), we get the Alfvén wave equation in spherical geometry

$$\frac{\partial^2 v_\phi}{\partial t^2} = v_A(r)^2\left(\frac{\partial^2 v_\phi}{\partial r^2} - \frac{2}{r}\frac{\partial v_\phi}{\partial r} + \frac{2}{r^2}v_\phi\right), \tag{13}$$

where $v_A(r) = B_0/r^2\sqrt{\rho}$. Finally, substituting $e^{i\omega t}$ for the time dependence, we get

$$r^2 v_\phi'' - 2r\, v_\phi' + (2 + \omega^2 r^2/v_A^2)v_\phi = 0, \tag{14}$$

where the primes denote radial derivatives. Equation (14) can be readily solved using standard mathematical packages on a personal computer. In Figure 10 we show a solution of equation (14) with the boundary conditions $v_\phi(1) = v_d = 0.02 v_A = 30.5$ km s^{-1} and $v_\phi'(1) = 0$ and with the parameters $\omega = 9.6$ ($\Rightarrow f = 3.33$ mHz), $\omega = 1$ ($\Rightarrow f = 0.35$ mHz), $B = 7$ G, and $T = 1.4 \times 10^6$ K, obtained with the Mathematica© software package. It is evident that the velocity amplitude of the wave increases rapidly with r. When $\omega = 9.6$, the increase is in agreement with equation (8). When $\omega = 1$, the asymptotic amplitude of the Alfvén waves is larger than the value predicted by equation (8). It is also evident that the wavelength of the Alfvén waves decreases with r. When lower-frequency Alfvén waves are launched into the model corona ($\omega = 1$) the maximal wave amplitude is about 30% larger than the higher-frequency wave amplitude. We have tested our 2.5-D MHD code by comparing the solutions for small-amplitude Alfvén waves (small nonlinearity) with the solution of equation (14) and found very good agreement.

Acknowledgments. We thank the referees for the valuable comments and suggestions that helped to improve this

paper. This work was supported by the NASA SR&T program, the Space Physics Theory program, and the HPCC program. The JPL/Caltech Cray Supercomputer used in this investigation was provided through funding by the NASA offices of Mission to Planet Earth, Aeronautics, and Space Science.

The Editor thanks Thomas E. Holzer and Keith MacGregor for their assistance in evaluating this paper.

References

Alazraki, G., and P. Couturier, Solar wind acceleration caused by the gradient of Alfvén wave pressure, *Astron. Astrophys., 13*, 380, 1971.

An, C.-H., S.T. Suess, R.L. Moore, and Z.E. Musielak, Reflection and trapping of Alfvén waves in a spherically symmetric stellar atmosphere, *Astrophys. J., 350*, 309, 1990.

Andreev, V.E., A.I. Efimov, L.N. Samozaev, M.K. Bird, Faraday rotation fluctuation spectra observed during solar occultation of the Helios spacecraft, in ***Solar Wind Eight,*** edited by Winterhalter D. et al., *AIP Conf. Proc. 382*, 34-37, 1996.

Barnes, A., Theory of magnetohydrodynamic waves: The WKB approximation revisited, *J. Geophys. Res., 97*, 12,105, 1992.

Belcher, J.W., Alfvénic wave pressures and the solar wind, *Astrophys. J., 168*, 509, 1971.

Belcher, J.W., and S. Olbert, Stellar winds driven by Alfvén waves, *Astrophys. J., 200*, 369, 1975.

Boynton G.C., and U. Torkelsson, Dissipation of non-linear Alfvén waves, *Astron. Astrophys., 308*, 299, 1996.

Charbonneau, P., and K.B. MacGregor, Stellar winds with non-WKB Alfvén waves, II, Wind models for cool, evolved stars, *Astrophys. J., 454*, 901, 1995.

Davila, J.M., A leaky magnetohydrodynamic waveguide model for the acceleration of high-speed solar wind, *Astrophys. J., 291*, 328, 1985.

Davila, J.M., Heating of the solar corona by the resonant absorption of Alfvén waves, *Astrophys. J., 317*, 514, 1987.

Denskat, K.U., and F.M. Neubauer, Statistical properties of low-frequency magnetic field fluctuations in the solar wind from 0.29 to 1.0 AU during solar minimum conditions: Helios 1 and Helios 2, *J. Geophys. Res., 87*, 2215, 1982.

Esser, R., E. Leer, S.R. Habbal, and G.L. Withbroe, A two-fluid solar wind model with Alfvén waves: Parameter study and application to observations, *J. Geophys. Res., 91*, 2950, 1986.

Esser, R., S.R. Habbal, W.A. Coles, and J.V. Hollweg, Hot protons in the inner corona and their effect on the flow properties of the solar wind, *J. Geophys. Res., 102*, 7063, 1997.

Grall, R.R., W.A. Coles, M.T. Klinglesmith, A.R. Breen, P.J.S. Williams, J. Markkanen, and R. Esser, Rapid acceleration of the polar solar wind, *Nature, 379*, 429, 1996.

Grappin, R., A. Mangeney, and E. Marsch, On the origin of solar wind MHD turbulence: Helios data revisited, *J. Geophys. Res., 95*, 8197, 1990.

Hassler, D.M., G.J. Rottman, E.C. Shoub, and T.E. Holzer, Line broadening of Mg X 609Å and 625Å coronal emission lines observed above the solar limb, *Astrophys. J., 348*, L77, 1990.

Heinemann, M., and S. Olbert, Non-WKB Alfvén waves in the solar wind, *J. Geophys. Res., 85*, 1311, 1980.

Hollweg, J.V., Alfvén waves in a two-fluid model of the solar wind, *Astrophys. J., 181*, 547, 1973.

Hollweg, J.V., On WKB expansions for Alfvén waves in the solar wind, *J. Geophys. Res., 95*, 14,873, 1990.

Holzer, T.E., and E. Leer, Conductive solar wind models in rapidly diverging flow geometries, *J. Geophys. Res., 85*, 4665, 1980.

Jacques, S.A., Momentum and energy transport by waves in the solar atmosphere and solar wind, *Astrophys. J., 215*, 942, 1977.

Klinglesmith, M.T., The polar solar wind from 2.5 to 40 solar radii: Results of intensity scintillation measurements, Ph.D. thesis, Univ. of Calif., San Diego, 1996.

Kopp, R.A., and T.E. Holzer, Dynamics of coronal hole regions, I, Steady polytropic flows with multiple critical points, *Sol. Phys., 49*, 43, 1976.

Krieger, A.S., A.F. Timothy, and E.C. Roelof, A coronal hole and its identification as the source of a high velocity solar wind stream, *Sol. Phys., 29*, 505, 1973.

Lau, Y.-T., and E. Siregar, Nonlinear Alfvén wave propagation in the solar wind, *Astrophys. J., 464*, 1054, 1996.

Leer, E., and T.E. Holzer, Energy addition in the solar wind, *J. Geophys. Res., 85*, 4681, 1980.

Linker, J.A., G. Van Hoven, and D.D. Schnack, A three-dimensional simulation of a coronal streamer, *Geophys. Res. Lett, 17*, 2281, 1990.

Lou, Y.-Q., Three-dimensional nonsteady compressible magnetohydrodynamic fluctuations in the solar-wind, *J. Geophys. Res., 98*, 11,483, 1993a.

Lou, Y.-Q., Propagation of three-dimensional Alfvén waves and its nonlinear effects in the solar wind, *J. Geophys. Res., 98*, 3563, 1993b.

Lou, Y.-Q., and R. Rosner, Reflection of Alfvén waves in stellar atmospheres: The case of open magnetic fields, *Astrophys. J., 424*, 429, 1994.

MacGregor, K.B., and P. Charbonneau, Stellar winds with non-WKB Alfven waves, 1, Wind models for solar coronal conditions, *Astrophys. J., 430*, 387, 1994.

Marsch, E., and C.-Y. Tu, On the radial evolution of MHD turbulence in the inner heliosphere, *J. Geophys. Res., 95*, 8211, 1990.

Mikić, Z., and J.A. Linker, The large-scale structure of the solar corona and the inner heliosphere, in *Solar Wind Eight*, edited by Winterhalter D. et al., *AIP Conf. Proc. 382*, 104-107, 1996.

Misawa, H., and M. Kojima, Dependence of velocity fluctuations on solar wind speeds from an IPS analysis method, in *Solar Wind Eight*, edited by Winterhalter D. et al., *AIP Conf. Proc. 382*, 113-116, 1996.

Neupert, W.M., and V. Pizzo, Solar coronal holes as sources of recurrent geomagnetic disturbances, *J. Geophys. Res., 79*, 3701, 1974.

Nolte, J.T., A.S. Krieger, A.F. Timothy, R. E. Gold, E.C. Roelof, G. Vaina, A.J. Lazarus, J.D. Sullivan, and P.S. McIntosh, Coronal holes as sources of solar wind, *Sol. Phys., 46*, 303, 1976.

Ofman, L., and J.M. Davila, Alfvén wave heating of coronal holes and the relation to the high-speed solar wind, *J. Geophys. Res., 100*, 23,413, 1995.

Ofman, L., and J.M. Davila, Solar wind acceleration by solitary waves in coronal holes, *Astrophys. J., 476*, 357, 1997a.

Ofman, L., and J.M. Davila, Do first results from SOHO UVCS indicate that the solar wind is accelerated by solitary waves?, *Astrophys. J., 476*, L51, 1997b.

Ofman, L., M. Romoli, G. Poletto, G. Noci, and, J.L. Kohl, UVCS observations of density fluctuations in the solar wind, *Astrophys. J., 491*, L111, 1997.

Ong, K.K., Z.E. Musielak, R. Rosner, S.T. Suess, and M.E. Sulkanen, Self-consistent and time-dependent solar wind models, *Astrophys. J., 474*, L143, 1997.

Orlando, S., Y.-Q. Lou, R. Rosner, and G. Peres, Propagation of three-dimensional Alfvén waves in a stratified, thermally conducting solar wind, *J. Geophys. Res., 101*, 24,443, 1996.

Orlando, S., Y.-Q. Lou, G. Peres, and R. Rosner, Alfvénic

fluctuations in fast and slow solar winds, *J. Geophys. Res., 102*, 24,139, 1997.

Parker, E.N., *Interplanetary Dynamical Processes*, Wiley-Intersci., New York, 1963.

Phillips, J.L., et al., Ulysses solar wind plasma observations from pole to pole, *Geophys. Res. Lett., 22*, 3301, 1995.

Steinolfson, R.S., and Y. Nakagawa, Dynamical response of the solar corona, II, Numerical simulations near the Sun, *Astrophys. J., 207*, 300, 1976.

Usmanov, A.V., A global numerical 3-D MHD model of the solar wind, *Sol. Phys., 146*, 377, 1993.

Velli, M., On the propagation of ideal, linear Alfven waves in radially stratified stellar atmospheres and winds, *Astron. Astrophys., 270*, 304, 1993.

Wagner, W.J., Coronal holes observed by OSO-7 and interplanetary magnetic sector structure, *Astrophys. J., 206*, 583, 1976.

Winterhalter, D., J.T. Gosling, S.R. Habbal, W.S. Kurth, M. Neugebauer (Eds.), *Solar Wind Eight, AIP Conf. Proc. 382*, 680 pp., 1996.

J. M. Davila and L. Ofman, Laboratory for Astronomy and Solar Physics, Code 682, NASA Goddard Space Flight Center, Greenbelt, MD 20771. (e-mail: davila@lindsay.gsfc.nasa.gov; Leon.Ofman@gsfc.nasa.gov)

(Received March 24, 1998; revised June 5, 1998; accepted June 5, 1998.)